Environmental Science & Technology

pubs.acs.org/est

Article

Significantly Accelerated Photochemical Perfluorooctanoic Acid Decomposition at the Air−Water Interface of Microdroplets

Kejian Li, Wenbo You, Wei Wang, Kedong Gong, Yangyang Liu, Longqian Wang, Qiuyue Ge, Xuejun Ruan, Jianpeng Ao, Minbiao Ji, and Liwu Zhang*

Cite This: *Environ. Sci. Technol.* 2023, 57, 21448−21458

Read Online

ACCESS | Metrics & More | Article Recommendations | Supporting Information

ABSTRACT: The efficient elimination of per- and polyfluoroalkyl substances (PFASs) from the environment remains a huge challenge and requires advanced technologies. Herein, we demonstrate that perfluorooctanoic acid (PFOA) photochemical decomposition could be significantly accelerated by simply carrying out this process in microdroplets. The almost complete removal of 100 and 500 μg/L PFOA was observed after 20 min of irradiation in microdroplets, while this was achieved after about 2 h in the corresponding bulk phase counterpart. To better compare the defluorination ratio, 10 mg/L PFOA was used typically, and the defluorination rates in microdroplets were tens of times faster than that in the bulk phase reaction system. The high performances in actual water matrices, universality, and scale-up applicability were demonstrated as well. We revealed in-depth that the great acceleration is due to the abundance of the air−water interface in microdroplets, where the reactants concentration enrichment, ultrahigh interfacial electric field, and partial solvation effects synergistically promoted photoreactions responsible for PFOA decomposition, as evidenced by simulated Raman scattering microscopy imaging, vibrational Stark effect measurement, and DFT calculation. This study provides an effective approach and highlights the important roles of air-water interface of microdroplets in PFASs treatment.

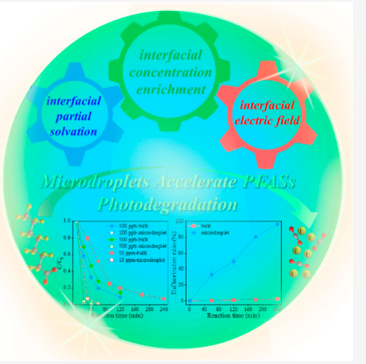

KEYWORDS: *PFASs, photochemistry, microdroplet, air−water interface, reaction acceleration*

INTRODUCTION

Per- and poly-fluoroalkyl substances (PFASs) have been widely used in the manufacturing of domestic and industrial materials, leading to significant dissemination in environments around the world.[1,2] The production and usage of perfluorooctanoic acid (PFOA) began in the 1940s, and it has become one of the most notorious PFASs, due to the extraordinary persistence, instant bioaccumulation, and high toxicity. The concentrations of PFOA in natural water environments are often in the range of ng/L to mg/L (e.g., drinking water, 4300 ng/L; surface water, 11,000 ng/L; wastewater, ppm level),[3,4] which are significantly higher than the EPA health advisory level in drinking water [70 ppt, total concentration of PFOA and perfluorooctanesulfonate (PFOS)], causing severe adverse effects on human health like cancer, birth defects, infertility, and immune dysfunction.[5−7] Highly efficient approaches are urgently required for PFOA and other PFASs elimination.

Adsorption is a simple method for pollutants removal, but the treatment is nondestructive and requires further disposal and adsorbents regeneration.[8,9] Besides, owing to the extremely high dissociation energy of C−F bonds and strong electronegativity of fluorine atoms, PFASs show negligible elimination in biodegradation and conventional advanced oxidation processes.[6] Photochemistry is considered as a promising approach for PFASs decomposition because which could integrate with the already widespread UV disinfection technologies.[10,11] The photochemical reductive decomposition initiated by hydrated electrons (e_{aq}^-) is generally conducted under anaerobic and alkaline conditions and requires the addition of sulfite and iodide.[12−14] However, the presence of sulfite in water is harmful to water quality, agricultural field, and human health (e.g., lung and brain cancer and headaches), and metal ions like Ca^{2+}, Mg^{2+}, and Fe^{3+} will form precipitates under alkaline conditions.[15,16] In comparison, UV photochemistry of the earth-abundant Fe^{3+} and NO_3^- could be operated under ambient conditions and is also studied for PFOA treatment.[17,18] However, the application of photochemical processes for PFOA elimination is limited by the low space-time-yield. Thus, it is of great significance to improve the photochemical treatment efficacy of PFASs-contaminated water through the exploiting of advanced strategies.

The C−F bonds in PFASs are of hydrophobic character while the carboxyl group is hydrophilic, making them preferentially accumulate at the gas−liquid interface and influence their adsorption, transport, and removal behav-

Received: July 11, 2023
Revised: October 3, 2023
Accepted: November 9, 2023
Published: December 4, 2023

iors.[5,19] It was reported that PFOA degradation mainly occurred at the interfacial region between microbubbles and bulk solution in ultrasonication and plasma treatment processes, because the enrichment of PFOA to the gas−liquid interface could improve the contact with reactive species.[20,21] Besides, Gu et al. found that the addition of alcohols could promote PFOA removal through improving the dispersion of PFOA in aqueous solution for efficient attack of active species.[22] Accordingly, the sluggish PFOA photochemical treatment in bulk solution might be due to the strong surface activity of PFOA and limited radicals attack. The partition extent of PFOA to the gas−liquid interface is proportional to the water surface area: the more abundant gas−liquid interface, the more significant interfacial enrichment.[23] Thus, it is anticipated that providing abundant gas−liquid interface would be favorable to the photochemical PFASs decomposition.

Microdroplet, as emerging chemical reactor, possesses extremely large surface-area-to-volume ratio (S/V) [namely, abundant air−water interface (AWI)],[24] which might be greatly conducive to the PFOA interfacial enrichment. Recent studies show that chemical reactions (e.g., organic synthesis,[25,26] $^{\bullet}OH$ production,[27] and SO_2 oxidation[28]) could be accelerated by 10−10^6 times in microdroplets compared to the corresponding bulk phase counterpart. Microdroplets could also induce spontaneous H_2O_2 formation,[29,30] $HAuCl_4$ reduction,[31] and I^- oxidation[32] in the absence of any external reagent. The intriguing behaviors were preliminarily attributed to the "on water catalysis" characteristic at microdroplet AWI.[33,34] Microdroplet AWI might provide an attractive reaction environment for PFASs photochemical decomposition but has not been explored, to the best of our knowledge.

Herein, we report that performing PFOA treatment by UV/$Fe(NO_3)_3$ photochemistry in a microdroplet reactor could significantly improve the decomposition efficacy and defluorination ratio, particularly for lower concentration PFOA and in smaller microdroplets. We thoroughly investigated the acceleration mechanisms through using simulated Raman scattering (SRS) spectra measurement, interfacial electric field study, and theoretical calculation. We further studied the treatment efficacy in natural water bodies and the feasibility of scale-up application. The results demonstrate that microdroplet photochemistry is highly efficient for environmental remediation.

MATERIALS AND METHODS

Microdroplets Generation and Photochemical Reaction. Microdroplets, generated from a homemade nebulizer, were collected on an as-prepared superhydrophobic quartz wafer that was placed about 3 cm away from the nebulizer outlet. The superhydrophobic treatment could give a water contact angle of 145 ± 2°, and the superhydrophobicity will not be influenced by UV light irradiation (Figure S1). As shown in Figure S2, the diameters of microdroplets were mainly in the range of 50−300 μm, and the microdroplet generation method was of great repeatability. To study the microdroplet size effects, the average diameter of microdroplets was controlled through changing the spraying times. Typical micrographs of microdroplets with obviously different average sizes are shown in Figure S3. After microdroplet generation, the quartz wafer was sealed into a custom-designed reaction chamber (Figure S4a) under high relative humidity conditions (RH > 93%). The details can be found in our previous study.[35] To avoid the impact of gas−liquid interface concentration enrichment of PFOA on microdroplet generation, the solution in nebulizer was mixed by 1 min oscillation before immediate spraying. The bulk phase reaction was carried out using a miniature beaker containing 5 mL solution with a thickness of ∼15 mm, and the top was covered with a quartz plate (Figure S4b).

The typical PFOA photodegradation experiments were conducted in the presence of 10 mM $Fe(NO_3)_3$ and 10 mg/L PFOA without pH adjusting (the original pH was about 2.4), under 254 nm UV light irradiation with a power density of ∼2.35 mW/cm^2. The microdroplet size negligibly changed after the photochemical reaction due to the low temperature and high relative humidity control (Figure S5). After a predesigned time interval, the microdroplets were collected and quantificationally diluted using 0.01 M HCl containing 5 vol % TBA for inhibiting iron precipitation and ceasing reactions, as well as for bulk phase reaction. The obtained samples were filtered with 0.45 μm polycarbonate membrane for analyses because the adsorption of PFASs on the polycarbonate membrane was negligible (as displayed in Figure S6).[36] All experiments were performed at least in triplicate, and the average values with standard deviation were reported. The detailed information about analytical methods was provided in Supporting Information.

Simulated Raman Scattering Spectra Measurements. The hydrophobic PFASs, Fe(III) species, and NO_3^- generally present water surface propensity, and the spatial separation of anions and cations could form electric double layer, resulting in reactants' concentration enrichment and strong electric field at the air−water interface.[37,38] In this study, micro-Raman-based technologies were applied to measure the interfacial concentration enrichment and ultrahigh electric field. The SRS spectra were recorded using a SRS microscope, and the details on the setup are described in previous works.[39,40] Because of the requirement for high concentrations of target molecules and laser-induced shrinkage of the pure $Fe(NO_3)_3$ droplet (as displayed in Figure S7), the mixtures of 1 M $NaNO_3$ and 30 mM $Fe(NO_3)_3$ with and without addition of 10 mg/L PFOA were employed for SRS measurements. The microdroplets were generated on a superhydrophobic coverslip using a homemade nebulizer and then the coverslip was flipped over onto the center perforated slide to form a sealed cell with the help of another coverslip and sealant, as shown in Figure S8. The closed chamber was held for 10 min to stabilize microdroplets under ambient condition. Because there is no Raman signal for Fe^{3+} and PFOA in aqueous solution (Figure S9), the Raman vibrational bands of NO_3^- ($\nu(NO_3^-)$) and H_2O ($\nu(H_2O)$) were measured at pump laser wavelengths of 940 and 776 nm, respectively. The internal standard method using H_2O as internal standard was applied to qualitatively evaluate the spatial distribution of NO_3^- concentration, namely, the SRS peak intensity ratio of $\nu(NO_3^-)$ to $\nu(H_2O)$ is proportional to the NO_3^- concentration.[41]

Interfacial Electric Field Measurements. The interfacial electric field in microdroplet was measured using micro-Raman spectroscopy based on the vibrational Stark effect.[37] Due to the high-sensitive local electric field response characteristic of C≡N bond and strong chemical adsorption of SCN^- on Au nanoparticles that are of surface-enhanced Raman scattering property,[42] the Raman spectra of SCN^- were detected at microdroplet interior and interface region (illustrated in Figure S10). The bulk solution containing NaSCN and Au nanoparticles in the presence and absence of $NaNO_3$ was prepared

https://doi.org/10.1021/acs.est.3c05470
Environ. Sci. Technol. 2023, 57, 21448−21458

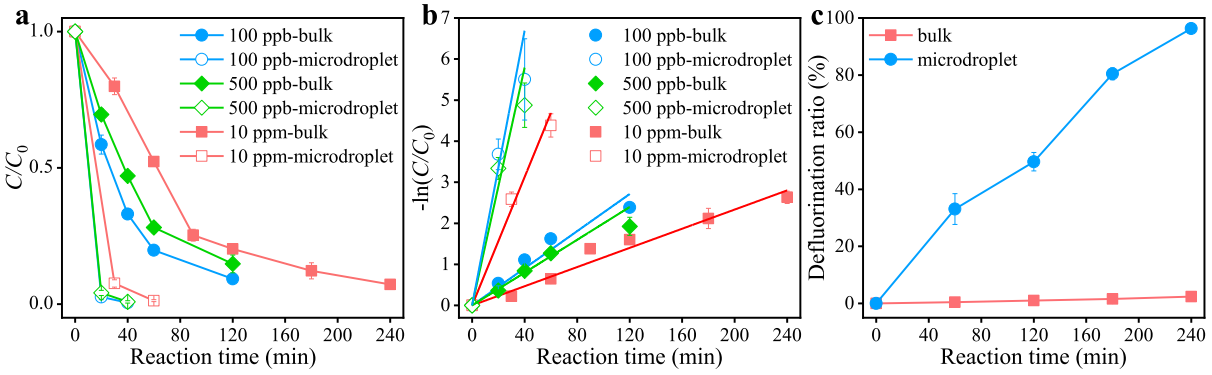

Figure 1. PFOA decomposition performance in bulk solution and microdroplets. (a) PFOA photochemical removal efficacy and (b) pseudo-first-order reaction kinetics fitting in the bulk phase and microdroplets. (c) Time dependence of defluorination ratio of 10 mg/L PFOA. Error bars represent the standard deviation from at least three independent experiments. Some of the standard deviations were smaller than the corresponding symbols.

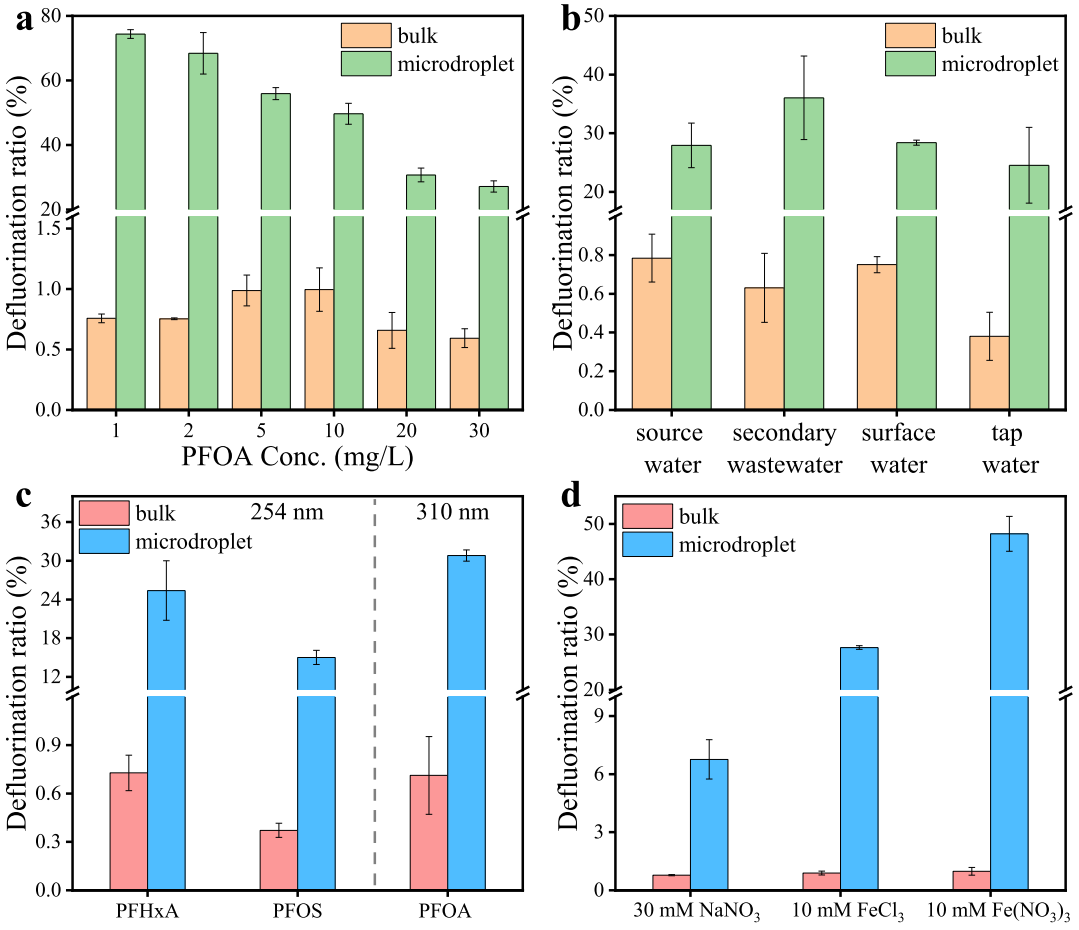

Figure 2. Impacts of experimental parameters and universality of accelerated photochemical defluorination. (a) Effects of the initial concentration of PFOA. (b) Defluorination ratios of PFOA in actual water matrices. (c) Defluorination ratio of PFHxA and PFOS in microdroplets and bulk phase. (d) Defluorination ratio of PFOA induced by different photoactive species. Unless otherwise stated, the experiments were conducted under 254 nm UV light irradiation and reaction time was 2 h, in the presence of 10 mg/L PFOA. Error bars represent the standard deviation from at least three independent experiments.

following the procedures, as shown in Supporting Information. Because Fe^{3+} can react with SCN^- (Figure S11),[43] it is infeasible to measure interfacial electric field in microdroplet containing Fe^{3+}.

Microdroplets were sprayed onto a superhydrophobic quartz wafer, which was then placed into a homemade flow cell (Figure S12). To suppress water evaporation, high-purity air with high relative-humidity (RH > 93%) was purged into the flow cell at a flow rate of 50 mL/min. The Raman spectra of C≡N bond (ν(C≡N)) were recorded using a XploRA Plus confocal Raman spectrometer (Jobin Yvon, HORIBA Gr, France) coupled with ×50 Olympus microscope objective and 785 nm excitation laser. The Raman signal was collected using a multichannel EMCCD device ranging from 2000 to 2200

https://doi.org/10.1021/acs.est.3c05470
Environ. Sci. Technol. 2023, 57, 21448−21458

cm^{-1}, with 2 spectrum accumulation at a 30 s acquisition time per spectrum. The electric field strength (E) is calculated from the following conversion equation (eq 1),[42] where $\Delta\nu(C\equiv N)$ is the difference value of detected Raman shift of $\nu(C\equiv N)$ between the microdroplet interior and interface.

$$E = (\Delta\nu(C \equiv N)/0.36) \times 10^6\ [(V/cm)/cm^{-1}] \quad (1)$$

RESULTS AND DISCUSSION

Accelerated PFOA Photochemical Decomposition in Microdroplets. The PFOA photochemical degradation kinetics induced by UV photolysis of $Fe(NO_3)_3$ were first investigated through monitoring PFOA concentration as photoreaction proceeded. The diffusion of PFOA from aqueous solution to gas phase was insignificant because PFOA mainly existed in the forms of deprotonated anions and Fe^{3+}-carboxylate chelates in the reaction system (discussed later). As shown in Figure 1a, with PFOA concentrations of 100 and 500 μg/L, the almost complete removal was achieved after only 20 min of irradiation in microdroplets. However, in bulk phase reaction, the corresponding removal efficacy was about 91.6 and 85.3% after 2 h. For high concentration PFOA with 10 mg/L, the treatment efficacy reached about 98.8 and 93.6% after 1 and 4 h of irradiation in microdroplets and bulk solution, respectively. Meanwhile, the corresponding TOC removal efficacy was around 55.8 and 1.7% with 4 h of photoirradiation in microdroplet and bulk phase systems (Figure S13), indicating that microdroplet photochemistry is highly sufficient for PFOA mineralization. The pseudo-first-order reaction kinetics fitting (Figure 1b and Table S1) determined that the reaction rate constants were improved by approximately 7 times in microdroplets compared to the corresponding bulk phase counterpart. Overall, the results indicate that microdroplets are essentially favorable to PFOA photochemical decomposition at concentrations of environmental and industrial levels.

The defluorination ratio was adopted to further evaluate the PFOA treatment performances, as the cleavage of C−F bonds and defluorination are critical for completely eliminating the adverse effects of PFOA.[44] To better detect defluorination, typically 10 mg/L PFOA was used. Figure 1c shows that the almost complete defluorination was achieved in microdroplets after 4 h of photoirradiation, which was approximately 40.6-fold greater than that in the corresponding bulk phase counterpart (96.3 vs 2.4%). In the absence of $Fe(NO_3)_3$ or PFOA, the detected concentrations of F^- were similar to the background value even after photoreaction (Figure S14), suggesting the efficient defluorination was actually induced by UV/$Fe(NO_3)_3$ photochemistry. The defluorination ratios of PFOA with various initial concentrations were further investigated. As shown in Figure 2a, in the bulk phase system, the defluorination ratio (<1%) was first raised and then declined with increasing PFOA initial concentration from 1 to 30 mg/L. The lower defluorination ratio at lower PFOA initial concentration might be because of the stronger interfacial concentration enrichment, which decreased the reaction opportunity with active species that were dominantly generated in the interior of bulk solution. In sharp contrast, in microdroplets, the defluorination ratio was continuously increased with decreasing the initial concentration of PFOA. The defluorination ratio reached about 74.4% in the case of 1 mg/L PFOA after 2 h photoirradiation, which was approximately 98.2-fold greater than that in the corresponding bulk phase counterpart. Besides, the enhancement factors were higher in the presence of lower PFOA concentration (Figure S15), suggesting that microdroplets are more promising for the treatment of PFOA with a concentration of environmental significance. The degradation rate and defluorination ratio obtained in microdroplets are significantly higher than those in previous studies (Table S2), demonstrating the great superiority of microdroplets on PFOA photochemical treatment.

Influences of $Fe(NO_3)_3$ Concentration and Actual Water Matrices. In both bulk phase and microdroplet systems, as shown in Figure S16a, the defluorination ratio was first increased and then decreased with an increment of $Fe(NO_3)_3$ concentration, and the highest defluorination ratio was observed in the presence of 10 mM $Fe(NO_3)_3$. In general, the production of reactive species responsible for PFOA decomposition would increase with increasing $Fe(NO_3)_3$ concentration. Nevertheless, the strengthened dimerization of $^{\bullet}NO_2$ probably can bring driving force to inhibit PFOA defluorination in the presence of excess NO_3^-.[45] In addition, Figure S16b shows that the enhancement factors on defluorination between microdroplets and bulk phase presented a volcano-type variation trend to the $Fe(NO_3)_3$ concentration, indicating that the inhibition effects of high concentration $Fe(NO_3)_3$ on PFOA photochemical removal were more evident in microdroplets than that in the bulk phase, probably owing to the strong NO_3^- concentration enrichment at AWI of microdroplet (discussed later).

The PFOA defluorination in real water matrices (tap water, source water, surface water, and secondary wastewater effluent; see Table S3 for water chemistry) spiked with 10 mg/L PFOA and 10 mM $Fe(NO_3)_3$ was further tested. Figure 2b shows that, after 2 h of photoirradiation, the PFOA defluorination in microdroplets was significantly higher than that in bulk phase reaction for the four actual water matrices, with the corresponding enhancement factor of 64.3, 35.6, 37.8, and 57.1. The results demonstrate that microdroplet reactors are highly efficient for PFOA treatment in actual water environments. Besides, it could be observed that the defluorination ratios in actual water matrices were lower than that in deionized water, which might be attributed to the coexistence of various inorganic and organic substances. As shown in Figure S17, the presence of common anions (SO_4^{2-}, Cl^-, $H_2PO_4^-$, and CO_3^{2-}) with concentration of 1 mM and humic acid of 10 mg/L inhibited PFOA photochemical defluorination in both microdroplet and bulk phase reaction, indicating the decrease in defluorination might be due to the competition for the reactive species.[4]

Universality. Furthermore, the photochemical defluorination performances of perfluorohexanoic acid (PFHxA) and PFOS were investigated. As shown in Figure 2c, after 2 h UV light irradiation, the defluorination ratios were about 25.4 and 15.1% in microdroplets for PFHxA and PFOS, respectively, which were about 35.2- and 41.6-fold greater than that in the corresponding bulk phase reaction (0.72 and 0.37%, respectively). Meanwhile, the removal efficacy of PFOS (98.2 vs 26.4%) and the desulfurization ratio (38.1 vs 4.5%) were also obviously higher in microdroplets than that in the corresponding bulk phase reaction (Figure S18). As shown in Figure 2d, the level of PFOA defluorination induced by UV/$NaNO_3$ and UV/$FeCl_3$ was also dramatically higher in microdroplets than in the corresponding bulk phase reaction.

https://doi.org/10.1021/acs.est.3c05470
Environ. Sci. Technol. 2023, 57, 21448−21458

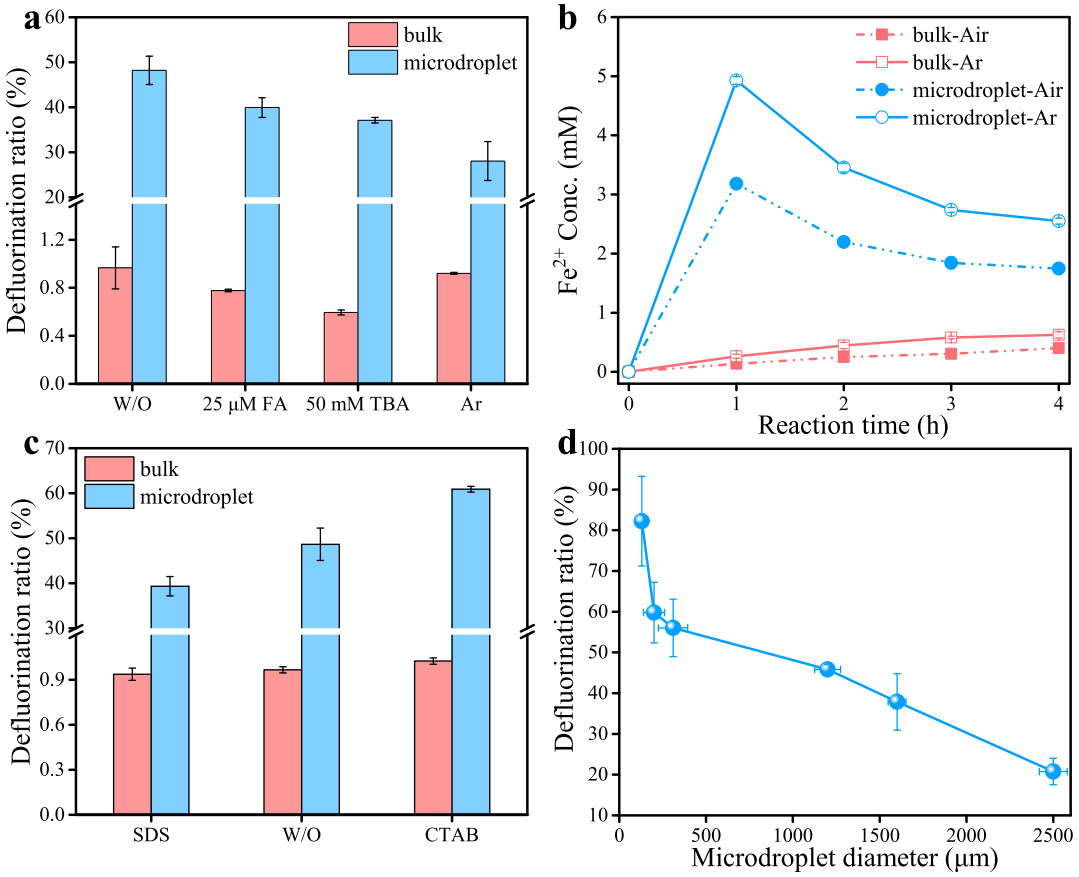

Figure 3. Reactive species and microdroplet size effect. (a) Effects of radical scavengers and reaction atmosphere on PFOA photochemical defluorination. (b) Fe^{2+} generation in microdroplets and bulk phase under air and Ar atmospheres. (c) Influences of CTAB and SDS on PFOA photochemical defluorination. (d) Microdroplet size effects on PFOA photochemical defluorination. Error bars represent the standard deviation from at least three independent sample.

Besides, Figure 2c shows that the defluorination ratio of 30.8% and enhancement factor of 43.2 were observed in microdroplets compared to the bulk phase counterpart, under 310 nm UV light irradiation that exists in the atmospheric layer.[46] Furthermore, the degradation efficacy of methyl orange (MO) and bisphenol A (BPA) by UV/$Fe(NO_3)_3$ photochemistry was also obviously higher in microdroplets than that in the bulk systems (Figure S19, experimental conditions are shown in Supporting Information). All the above results demonstrate that the microdroplet reactor is highly sufficient for environmental pollutants treatment, and microdroplet photochemistry would provide important implications in the understanding of atmospheric chemistry.

Acceleration Mechanism Study. As displayed in Figure 3a, the addition of 25 μM ferulic acid (FA, $^{\bullet}NO_2$ scavenger) obviously inhibited PFOA defluorination, indicating the crucial roles of $^{\bullet}NO_2$ generated from NO_3^- photolysis in PFOA treatment.[45,47] The addition of 50 mM tertiary butanol (TBA, $^{\bullet}OH$ quencher) also suppressed PFOA defluorination, implying the contributions of $^{\bullet}OH$ to PFOA decomposition. Although $^{\bullet}OH$ cannot directly attack the PFOA molecule, it could promote defluorination through reacting with degradation intermediates.[45,47] Figure S20 shows that the inhibition effects of FA and TBA on PFOA photochemical defluorination were more significant in the bulk phase than that in microdroplets, probably because the production of $^{\bullet}NO_2$ and $^{\bullet}OH$ through UV photolysis of $Fe(NO_3)_3$ was enhanced in microdroplets.

Under UV light irradiation, Fe(III)-containing species, mainly in the forms of $[C_nF_{2n+1}COO\text{-}Fe]^{2+}$, $Fe(OH)^{2+}$, and $[Fe(H_2O)_6]^{3+}$, would occur ligand-to-metal charge transfer (LMCT) process to contribute to PFOA photodegradation (reactions shown in Supporting Information).[45,48] As shown in Figure 3b, Fe^{2+} production in microdroplets was significantly higher than that in the bulk phase, indicating that the LMCT processes were faster in microdroplets. It could also be observed that the photolysis of Fe(III)-containing species became sluggish in microdroplets as photoreaction proceeded. Under an Ar environment, PFOA photochemical defluorination was inhibited while Fe^{2+} generation was improved in both microdroplet and bulk phase systems (Figure 3a,b). The results suggest that O_2 plays roles in PFOA photodegradation, particularly in microdroplets with highly sufficient O_2 availability.[49] Meanwhile, the presence of 1 mM p-BQ (a typical quencher of $O_2^{\bullet-}$) slightly decreased the photochemical defluorination in microdroplets (Figure S21a), indicating that $O_2^{\bullet-}$ played a negligible role in the PFOA photodegradation and suggesting that O_2 contributed to PFOA decomposition mainly through participating Fe^{2+} reoxidation and radical chain reactions. Besides, in the bulk phase system, the continuous purge of high-purity O_2 increased the defluorination ratio by about 3.6 times, while the defluorination in microdroplets was not significantly influenced by O_2 pure (Figure S21b). Moreover, the increment of light irradiation intensity also

https://doi.org/10.1021/acs.est.3c05470
Environ. Sci. Technol. 2023, 57, 21448−21458

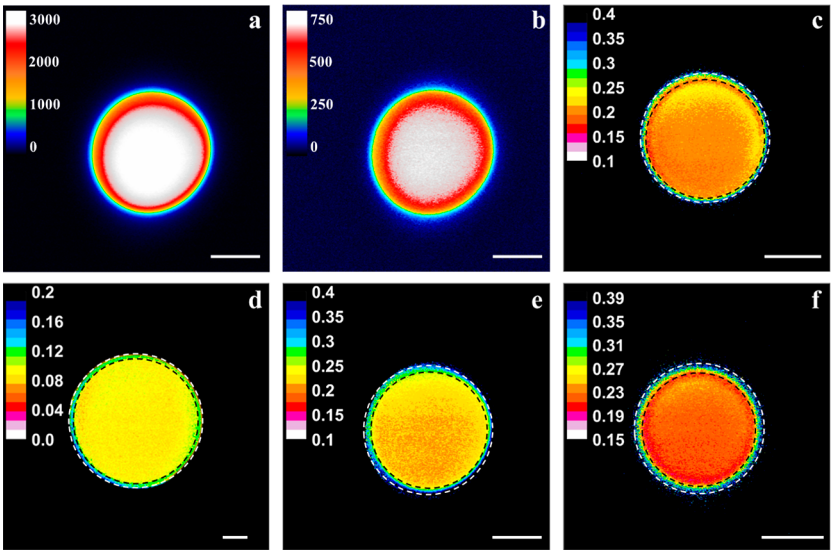

Figure 4. Concentration enrichment at AWI. The measured SRS spectra of (a) $\nu(H_2O)$ and (b) $\nu(NO_3^-)$ in a 49 μm-diameter-microdroplet in the presence of 10 mg/L PFOA, respectively. (c) SRS peak intensity ratios of $\nu(NO_3^-)$ to $\nu(H_2O)$ in a 46 μm-diameter microdroplet in the absence of PFOA. (d–f) SRS peak intensity ratios of $\nu(NO_3^-)$ to $\nu(H_2O)$ in microdroplet with size of about 110, 49, and 40 μm in the presence of 10 mg/L PFOA, respectively. The areas between black and white dashed lines represent the NO_3^- concentration enrichment regions. All the scale bar is 20 μm.

negligibly impacted photochemical defluorination in the bulk solution (Figure S21c). Therefore, the different physical characteristics (O_2 availability and light irradiation intensity) between microdroplets and bulk solution were not considerable reasons behind the significantly accelerated PFOA decomposition. In other words, the air–water interface of the microdroplet with special physicochemical properties might play critical roles in the acceleration.

To verify the important roles of the gas–liquid interface in PFOA photochemical decomposition, the effects of CTAB (cationic surfactant) and SDS (anionic surfactant) on defluorination were investigated. Because PFOA is an anionic surfactant, its gas–liquid interface accumulation would be strengthened by attractive force between anionic and cationic surfactants, but the concentration enrichment would be weakened due to the competing adsorption for AWI between two anionic surfactants.[50,51] As shown in Figure 3c, in both microdroplet and bulk phase systems, the defluorination was improved with addition of CTAB, while it was suppressed by introducing SDS. Meanwhile, the impacts of CTAB and SDS on PFOA photochemical defluorination were more significant in microdroplets than that in the bulk phase. The S/V of microdroplets is orders of magnitude larger than that of bulk solution (e.g., S/V = 0.03 μm^{-1} for 200 μm-diameter microdroplet and S/V = 6.3×10^{-4} μm^{-1} for bulk phase in this study), which is favorable to the AWI concentration enrichment. Accordingly, PFOA photochemical decomposition would mainly occur at microdroplet AWI.

The size effects of the microdroplet on PFOA photochemical defluorination were further studied to show the influences of AWI abundance. Figure 3d shows that, after 2 h photoreaction, the defluorination ratios were increased from ~20.7 to ~82.2% with decreasing average diameter of the microdroplet from around 2500 to 130 μm. With decreasing microdroplet size, the specific surface area of microdroplet would increase. The positive correlation between microdroplet S/V and defluorination ratio further confirms the dictating roles of microdroplet AWI in PFOA photodegradation.[52] AWI would provide unique reaction environment that is obviously distinct from the aqueous phase,[34,37,53] which probably can alter thermodynamics and kinetics of photoreactions responsible for PFOA decomposition. Accordingly, the roles of microdroplet AWI in accelerating photochemical defluorination were further investigated.

Reactant Concentration Enrichment at AWI. Undoubtedly, the hydrophobic PFOA could be intrinsically enriched at the air–water interface.[23] Besides, Allen et al. have reported the AWI accumulation characteristic of Fe(III) species and Chen et al. found the water surface-enriched nonanoic acid could attract Fe(III) to the air–water interface through chelation interaction.[54,55] Therefore, Fe(III)-containing species would be enriched at the AWI of microdroplets. NO_3^- also presents water surface affinity and the Coulombic attraction between NO_3^- and Fe(III)-containing species might enhance their concentration enrichment.[56,57] To verify the reactant concentration enrichment at microdroplet AWI, the spatial distribution of NO_3^- concentration in microdroplets was qualitatively investigated through SRS measurements. Figure 4a, b and Figure S22a,b represent the SRS spectra of $\nu(H_2O)$ and $\nu(NO_3^-)$ in individual microdroplet with a diameter of about 49 μm in the presence of PFOA and with a size of around 46 μm in the absence of PFOA, respectively. The SRS peak intensities were decreased as measuring from microdroplet interior to the air–water interface because the number of excited molecules gradually decreased.[58] Figure 4c–f and Figure S22c,d show that the SRS peak intensity ratios of $\nu(NO_3^-)$ to $\nu(H_2O)$ were distinctly larger at AWI of microdroplets with varying diameters, demonstrating the strong concentration enrichment of NO_3^- at interfacial region. Moreover, as displayed in Figure 5a, the volume fractions of the NO_3^- concentration enrichment region were larger in the presence of PFOA and in smaller microdroplets, confirming PFOA strengthened interfacial reactants concentration enrichment and indicating the concentration enrichment would be stronger with decreasing microdroplet size. Figure 2d shows that in microdroplets, the

https://doi.org/10.1021/acs.est.3c05470
Environ. Sci. Technol. 2023, 57, 21448–21458

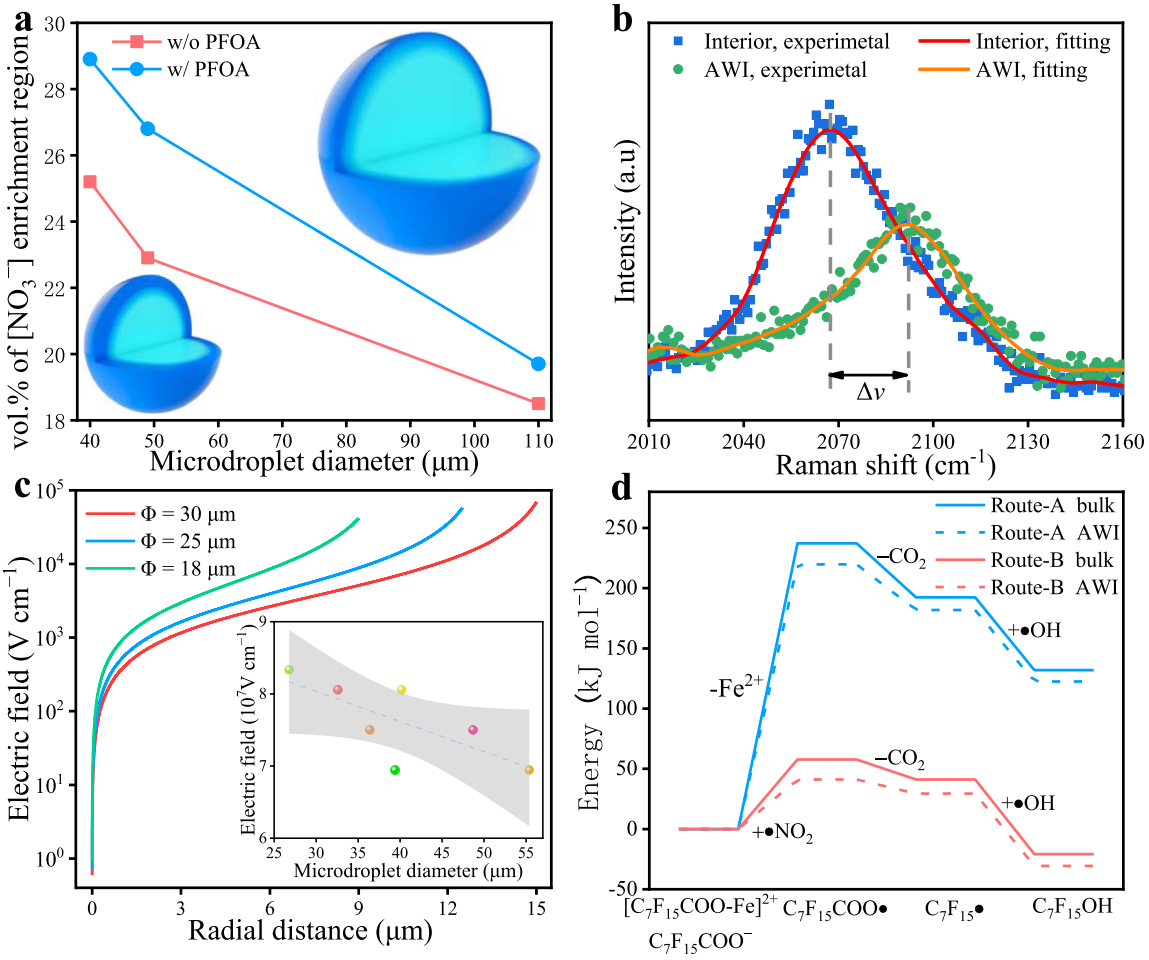

Figure 5. Ultrastrong electric field and reduced reaction energy barrier at the microdroplet AWI. (a) Volume fraction of the NO_3^- concentration enrichment region (interfacial blue color region) in microdroplets with and without 10 mg/L PFOA. (b) Raman spectra of ν(C═N) measured in a $NaNO_3$ microdroplet interior and at interface. Microdroplet size (Φ), ~55 μm. (c) Simulated microdroplet electric field strength. The inset is experimentally measured electric field strength in microdroplets with varying diameters. (d) Scheme of potential energy surface for PFOA photodegradation processes in bulk solution and at microdroplet AWI.

defluorination ratio and enhancement factor induced by UV/$Fe(NO_3)_3$ (48.2% and 49.9) were much higher than the sum of values obtained from UV/$NaNO_3$ (6.8% and 8.6) and UV/$FeCl_3$ (27.6% and 31.1), but which was not observed in the corresponding bulk phase counterpart. The results verify the synergistic effects of NO_3^- and Fe^{3+} on PFOA photodegradation in microdroplets, probably due to the interfacial Coulombic attraction force.

Ultrastrong Interfacial Electric Field. There may exist a strong electric field at microdroplet AWI due to the charge separation in the electric double layer,[59−61] which may influence the reactions at AWI. In this study, we measured the interfacial electric field in microdroplets containing $NaNO_3$ based on the vibrational Stark effect.[42,62] As displayed in Figure 5b, in a ~55 μm-diameter-microdroplet, compared to the Raman peak of ν(C≡N) measured in microdroplet interior, the obvious blue shift was observed for that detected at AWI (2066.3 vs 2090.4 cm^{-1}), indicating the existence of an ultrastrong interfacial electric field in the microdroplet. According to the conversion formula, the interfacial electric field strength was about 6×10^7 V/cm. Meanwhile, it was found that (inset in Figure 5c) the strength of the interfacial electric field was stronger in smaller microdroplets. Theoretical simulations further support that the interfacial electric field would be strengthened with decreasing microdroplet size (Figure 5c).[63] Although the interfacial electric field in microdroplets containing $Fe(NO_3)_3$ could not be experimentally measured due to the side reactions between SCN^- and Fe^{3+}, the ultrahigh interfacial electric field would also exist because of the intrinsic charges separation at AWI.[60,61] The ultrahigh electric field can lower the transition state barrier or raise the reactant state energy through bond activation,[59,64] which would contribute to the significant accelerations on PFOA photochemical decomposition.

Decreased Reaction Energy Barrier at AWI. For elucidating the reaction energy barriers (ΔE) of treatment processes responsible for PFOA decomposition at microdroplet AWI and in bulk solution, possible PFOA degradation pathways were investigated. Based on the detected short-chain perfluorocarboxylic acids (e.g., PFHpA, PFHxA, PFPeA, PFBA, PFPrA, and TFA), PFOA decomposition might follow decarboxylation−hydroxylation−elimination−hydrolysis (DHEH) processes, as illustrated in Figure 6a and the detailed descriptions could be found in Supporting Information.[6,65] Noticeably, PFPrA and TFA were readily detected in microdroplets after 2 h of photoirradiation, while they were not measured in the bulk phase reaction system even after 4 h (Figure S23). Besides, the hydrophobicity of PFCAs becomes comparatively weak with

https://doi.org/10.1021/acs.est.3c05470
Environ. Sci. Technol. 2023, 57, 21448−21458

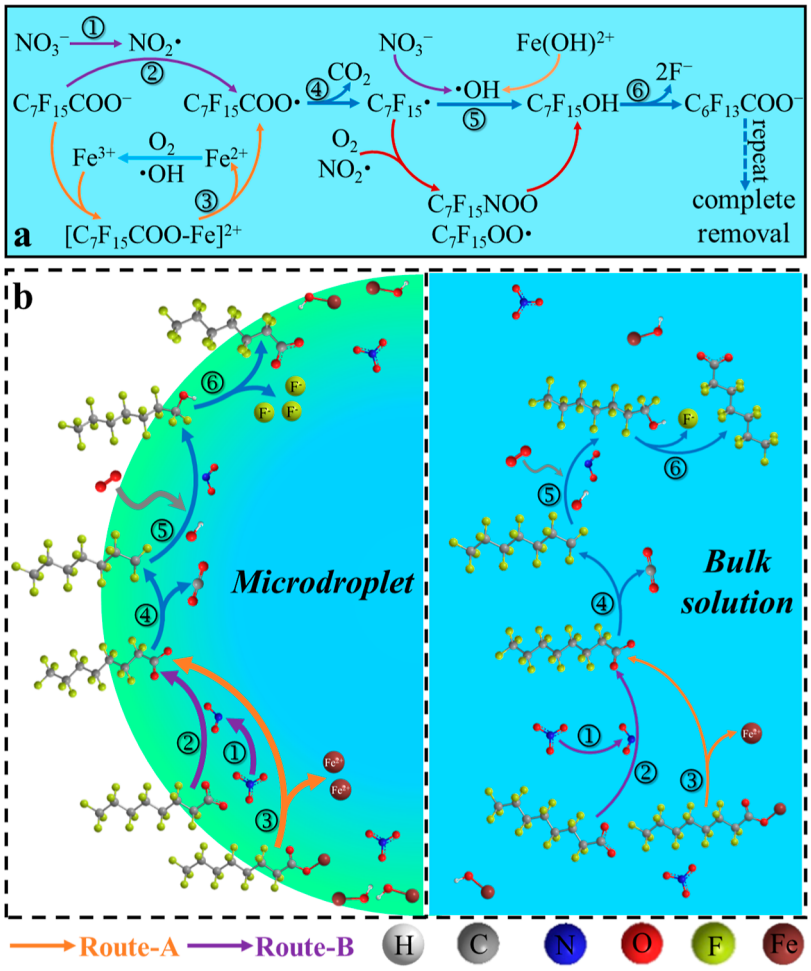

Figure 6. Degradation pathways and acceleration mechanisms. (a) Possible PFOA decomposition pathways induced by UV/Fe$(NO_3)_3$. (b) Scheme of mechanisms for significantly accelerated PFOA photodegradation.

shortening carbon chain length,[66] which probably can weaken interfacial concentration enrichment of reactants and slow Fe^{2+} production in microdroplets.

At AWI, molecules would be in partial solvation state rather than full solvation that exists in bulk solution, which could decrease energy barrier of desolvation and enhance reactivity of reactants.[34,53] Accordingly, the ΔE of photoreactions responsible for PFOA decomposition might be altered, which was then investigated through DFT calculation (details are shown in Supporting Information). As shown in Figure 5d, the ΔE of Route-A and Route-B was about 219.8 and 41.4 kJ/mol at microdroplet AWI, respectively, which was obviously lower than the ΔE in bulk phase reaction (237.1 and 57.8 kJ mol^{-1}, respectively), favoring the $C_7F_{15}COO^{\bullet}$ generation. The enhanced Fe^{2+} production in microdroplets compared to the bulk phase counterpart might be due to the lowered reaction energy barrier of the LMCT processes at microdroplet AWI. The ΔE of subsequent radical chain reactions was negative and almost similar between microdroplet AWI and bulk solution, indicating that the formation of $C_7F_{15}COO^{\bullet}$ was the rate-determining step for PFOA decomposition. In addition, Wingen et al. found that NO_3^- photolysis could be dramatically improved at the water surface because NO_3^- experienced weakened solvent cage effects, which would benefit to $^{\bullet}NO_2$ generation and PFOA decomposition.[67] Therefore, the predominant photoreactions responsible for PFOA degradation were both kinetically and thermodynamically more favorable at microdroplet AWI than in bulk solution, resulting in significant accelerations on photochemical defluorination. The acceleration mechanisms were then illustrated in Figure 6b. The hydrophobic nature of PFOA and the surface affinity of Fe^{3+} and NO_3^- promote photoreactions to predominantly occur at the AWI of microdroplets. In the microdroplet, the ultrahigh interfacial electric field and partial solvation effects at AWI lowered reaction energy barriers of the rate-determining step of $C_7F_{15}COO^{\bullet}$ formation, thus leading to significant accelerations on PFOA elimination.

Scale-Up Application. Finally, as a proof-of-concept, the practical applicability of microdroplet photochemistry for PFASs treatment was demonstrated through using an electrical nebulizer for microdroplets generation (setup shown in Figure S24). The removal efficacy and defluorination ratio of PFOA were approximately 3.8- and 14.4-fold greater than those in the corresponding bulk phase reaction system, respectively (Figure S25). The PFOA decomposition performances obtained from electrical nebulization were lower than that from the above static experiments, probably because the real photochemical reaction time was much shorter than the light irradiation time due to the settlement of microdroplets. Besides, as shown in Figure S26, there was negligible PFOA degradation and defluorination observed in microdroplets during electrical nebulization in the absence of UV light irradiation and

https://doi.org/10.1021/acs.est.3c05470
Environ. Sci. Technol. 2023, 57, 21448−21458

$Fe(NO_3)_3$, indicating that the significant PFOA decomposition was induced by microdroplet photochemistry. The potential economic cost of the bench scale setup for applying microdroplet photochemistry to treat PFASs-containing wastewater is discussed in Supporting Information. Moreover, for incorporating microdroplet process into current UV-based water treatment technologies, it would be feasible to use commercial water sprinkler for microdroplets generation and a reaction tank could be designed to make it easier to reflux condensates for secondary treatment and to provide UV light irradiation efficiently.

ENVIRONMENTAL IMPLICATIONS

For the first time, microdroplets were demonstrated to be effective for the photochemical treatment of recalcitrant PFASs with various concentrations and in actual water matrices. The defluorination ratio was improved by tens of times in microdroplets compared with the corresponding bulk phase counterpart. The acceleration mechanisms were experimentally and theoretically investigated, showing that PFASs decomposition mainly occurred at microdroplet AWI due to the water surface affinity of reactants, as verified by SRS measurements. The ultrahigh interfacial electric field and partial solvation effects synergistically decreased reaction energy barriers and thus accelerated photochemical treatment. The universal efficacy of enhanced PFASs photochemical decomposition in microdroplets was demonstrated along with its potential for large-scale application. This study provides an innovative technology for environmental remediation and highlights the important role of AWI in environmental chemistry.

The e_{aq}^-, I^-, and Cl^- tend to accumulate at the gas−liquid interface as well,[61,68,69] thus the PFASs photochemical treatment induced by other photochemical processes (e.g., UV/I^-, UV/Cl^-, and even semiconductor photocatalysis) probably can also be accelerated by using microdroplet reactors. Besides, owing to the significantly abundant AWI, microdroplets would be of great promise for eliminating other hydrophobic micropollutants like phenolic compounds and alkanes.[70,71] In natural environments, the microlayer of lakes and oceans, as well as the atmospheric aerosols and water droplets generated from bubble burst at water surfaces,[72] provide a prevalent air−water interface for concentration enrichment of PFASs and may display different reaction environment from the bulk interior. The fate and transport of PFASs in natural water bodies and atmosphere will be influenced by air−water interface chemistry and should be re-evaluated based on the current study, as well as the redox cycle of Fe(II)/Fe(III).

ASSOCIATED CONTENT

Supporting Information

The Supporting Information is available free of charge at https://pubs.acs.org/doi/10.1021/acs.est.3c05470.

Materials, analytic methods, Au nanoparticles synthesis, theoretical calculation, electric field simulation, scale-up experiments, and chemical reactions. Links to the Supporting Information for will be provided upon receipt (PDF)

AUTHOR INFORMATION

Corresponding Author

Liwu Zhang − *Department of Environmental Science and Engineering, Fudan University, Shanghai 200433, People's Republic of China; Shanghai Key Laboratory of Atmospheric Particle Pollution and Prevention, Fudan University, Shanghai 200433, People's Republic of China; Shanghai Institute of Pollution Control and Ecological Security, Shanghai 200092, People's Republic of China;* orcid.org/0000-0002-0765-8660; Email: zhanglw@fudan.edu.cn

Authors

Kejian Li − *Department of Environmental Science and Engineering, Fudan University, Shanghai 200433, People's Republic of China; Shanghai Key Laboratory of Atmospheric Particle Pollution and Prevention, Fudan University, Shanghai 200433, People's Republic of China; Shanghai Institute of Pollution Control and Ecological Security, Shanghai 200092, People's Republic of China*

Wenbo You − *Department of Environmental Science and Engineering, Fudan University, Shanghai 200433, People's Republic of China*

Wei Wang − *Department of Environmental Science and Engineering, Fudan University, Shanghai 200433, People's Republic of China*

Kedong Gong − *Department of Environmental Science and Engineering, Fudan University, Shanghai 200433, People's Republic of China;* orcid.org/0000-0003-2460-4370

Yangyang Liu − *Department of Environmental Science and Engineering, Fudan University, Shanghai 200433, People's Republic of China*

Longqian Wang − *Department of Environmental Science and Engineering, Fudan University, Shanghai 200433, People's Republic of China*

Qiuyue Ge − *Department of Environmental Science and Engineering, Fudan University, Shanghai 200433, People's Republic of China*

Xuejun Ruan − *Department of Environmental Science and Engineering, Fudan University, Shanghai 200433, People's Republic of China*

Jianpeng Ao − *State Key Laboratory of Surface Physics, Department of Physics, Fudan University, Shanghai 200433, People's Republic of China*

Minbiao Ji − *State Key Laboratory of Surface Physics, Department of Physics, Fudan University, Shanghai 200433, People's Republic of China*

Complete contact information is available at: https://pubs.acs.org/10.1021/acs.est.3c05470

Notes

The authors declare no competing financial interest.

ACKNOWLEDGMENTS

The authors gratefully acknowledge financial support from National Natural Science Foundation of China (No. 22176036, No. 21976030, and No. 22006020) and the Natural Science Foundation of Shanghai (No. 19ZR1471200).

REFERENCES

(1) Trojanowicz, M.; Bojanowska-Czajka, A.; Bartosiewicz, I.; Kulisa, K. Advanced oxidation/reduction processes treatment for aqueous perfluorooctanoate (PFOA) and perfluorooctanesulfonate (PFOS)-A review of recent advances. *Chem. Eng. J.* **2018**, *336*, 170−199.

(2) Evich, M. G.; Davis, M. J. B.; McCord, J. P.; Acrey, B.; Awkerman, J. A.; Knappe, D. R. U.; Lindstrom, A. B.; Speth, T. F.; Tebes-Stevens, C.; Strynar, M. J.; et al. Per- and polyfluoroalkyl substances in the environment. *Science* **2022**, *375* (6580), No. eabg9065.
(3) Long, M.; Donoso, J.; Bhati, M.; Elias, W. C.; Heck, K. N.; Luo, Y.-H.; Lai, Y. S.; Gu, H.; Senftle, T. P.; Zhou, C.; et al. Adsorption and reductive defluorination of perfluorooctanoic acid over palladium nanoparticles. *Environ. Sci. Technol.* **2021**, *55* (21), 14836−14843.
(4) Zhang, H.; Li, P.; Zhang, A.; Sun, Z.; Liu, J.; Héroux, P.; Liu, Y. Enhancing interface reactions by introducing microbubbles into a plasma treatment process for efficient decomposition of PFOA. *Environ. Sci. Technol.* **2021**, *55* (23), 16067−16077.
(5) Abraham, J. E. F.; Mumford, K. G.; Patch, D. J.; Weber, K. P. Retention of PFOS and PFOA mixtures by trapped gas bubbles in porous media. *Environ. Sci. Technol.* **2022**, *56*, 15489−15498.
(6) Wen, Y.; Rentería-Gómez, Á.; Day, G. S.; Smith, M. F.; Yan, T.-H.; Ozdemir, R. O. K.; Gutierrez, O.; Sharma, V. K.; Ma, X.; Zhou, H.-C. Integrated photocatalytic reduction and oxidation of perfluorooctanoic acid by metal-organic frameworks: Key insights into the degradation mechanisms. *J. Am. Chem. Soc.* **2022**, *144* (26), 11840−11850.
(7) Trang, B.; Li, Y.; Xue, X.; Ateia, M.; Houk, K. N.; Dichtel, W. R. Low-temperature mineralization of perfluorocarboxylic acids. *Science* **2022**, *377* (6608), 839−845.
(8) Liu, X.; Zhu, C.; Yin, J.; Li, J.; Zhang, Z.; Li, J.; Shui, F.; You, Z.; Shi, Z.; Li, B.; et al. Installation of synergistic binding sites onto porous organic polymers for efficient removal of perfluorooctanoic acid. *Nat. Commun.* **2022**, *13* (1), 2132.
(9) Wei, Z.; Xu, T.; Zhao, D. Treatment of per- and polyfluoroalkyl substances in landfill leachate: Status, chemistry and prospects. *Environ. Sci.: Water Res. Technol.* **2019**, *5* (11), 1814−1835.
(10) Yuan, F.; Hu, C.; Hu, X.; Qu, J.; Yang, M. Degradation of selected pharmaceuticals in aqueous solution with UV and UV/H_2O_2. *Water Res.* **2009**, *43* (6), 1766−1774.
(11) Metz, J.; Zuo, P.; Wang, B.; Wong, M. S.; Alvarez, P. J. J. Perfluorooctanoic acid degradation by UV/chlorine. *Environ. Sci. Technol. Lett.* **2022**, *9* (8), 673−679.
(12) Sun, Z.; Zhang, C.; Chen, P.; Zhou, Q.; Hoffmann, M. R. Impact of humic acid on the photoreductive degradation of perfluorooctane sulfonate (PFOS) by UV/iodide process. *Water Res.* **2017**, *127*, 50−58.
(13) Gao, J.; Liu, Z.; Chen, Z.; Rao, D.; Che, S.; Gu, C.; Men, Y.; Huang, J.; Liu, J. Photochemical degradation pathways and near-complete defluorination of chlorinated polyfluoroalkyl substances. *Nat. Water.* **2023**, *1* (4), 381−390.
(14) Liu, Z.; Chen, Z.; Gao, J.; Yu, Y.; Men, Y.; Gu, C.; Liu, J. Accelerated degradation of perfluorosulfonates and perfluorocarboxylates by UV/sulfite + iodide: Reaction mechanisms and system efficiencies. *Environ. Sci. Technol.* **2022**, *56* (6), 3699−3709.
(15) Khan, M. R.; Wabaidur, S. M.; Azam, M.; AlAmmari, A. M. Assessment of inorganic ion in drinking water using new method based on ultra-performance liquid chromatography-mass spectrometry. *J. King Saud Univ. Sci.* **2020**, *32* (4), 2329−2335.
(16) Yin, L. Q.; Yuan, D. X.; Zhang, M. Determination of sulfite in water samples by flow injection analysis with fluorescence detection. *Chin. Chem. Lett.* **2010**, *21* (12), 1457−1461.
(17) Wang, Y.; Zhang, P.; Pan, G.; Chen, H. Ferric ion mediated photochemical decomposition of perfluorooctanoic acid (PFOA) by 254 nm UV light. *J. Hazard. Mater.* **2008**, *160* (1), 181−186.
(18) Li, A.; Zhang, Z.; Li, P.; Cai, L.; Zhang, L.; Gong, J. Nitrogen dioxide radicals mediated mineralization of perfluorooctanoic acid in aqueous nitrate solution with UV irradiation. *Chemosphere* **2017**, *188*, 367−374.
(19) Schaefer, C. E.; Culina, V.; Nguyen, D.; Field, J. Uptake of poly- and per-fluoroalkyl substances at the air-water interface. *Environ. Sci. Technol.* **2019**, *53* (21), 12442−12448.
(20) Obo, H.; Takeuchi, N.; Yasuoka, K. Decomposition of perfluorooctanoic acid in water using multiple plasma generation. *IEEE Trans. Plasma Sci.* **2013**, *41* (12), 3634−3639.
(21) Vecitis, C. D.; Park, H.; Cheng, J.; Mader, B. T.; Hoffmann, M. R. Enhancement of perfluorooctanoate and perfluorooctanesulfonate activity at acoustic cavitation bubble interfaces. *J. Phys. Chem. C* **2008**, *112* (43), 16850−16857.
(22) Chen, Z.; Teng, Y.; Wang, W.; Hong, R.; Huang, L.; Wang, X.; Zhu, F.; Li, H.; Hao, S.; Wu, B.; et al. Enhanced UV photoreductive destruction of perfluorooctanoic acid in the presence of alcohols: Synergistic mechanism of hydroxyl radical quenching and solvent effect. *Appl. Catal., B* **2022**, *316*, 121652.
(23) Costanza, J.; Arshadi, M.; Abriola, L. M.; Pennell, K. D. Accumulation of PFOA and PFOS at the air-water interface. *Environ. Sci. Technol. Lett.* **2019**, *6* (8), 487−491.
(24) Bzdek, B. R.; Reid, J. P.; Cotterell, M. I. Open questions on the physical properties of aerosols. *Chem. Commun.* **2020**, *3* (1), 105.
(25) Huang, K.; Wei, Z.; Cooks, R. G. Accelerated reactions of amines with carbon dioxide driven by superacid at the microdroplet interface. *Chem. Sci.* **2021**, *12* (6), 2242−2250.
(26) Müller, T.; Badu-Tawiah, A.; Cooks, R. G. Accelerated Carbon−Carbon Bond-Forming Reactions in Preparative Electrospray. *Angew. Chem., Int. Ed.* **2012**, *51* (47), 11832−11835.
(27) Zhang, D.; Wang, J.; Chen, H.; Gong, C.; Xing, D.; Liu, Z.; Gladich, I.; Francisco, J. S.; Zhang, X. Fast hydroxyl radical generation at the air-water interface of aerosols mediated by water-soluble $PM_{2.5}$ under ultraviolet A radiation. *J. Am. Chem. Soc.* **2023**, *145* (11), 6462−6470.
(28) Angle, K. J.; Neal, E. E.; Grassian, V. H. Enhanced rates of transition-metal-ion-catalyzed oxidation of S(IV) in aqueous aerosols: Insights into sulfate aerosol formation in the atmosphere. *Environ. Sci. Technol.* **2021**, *55* (15), 10291−10299.
(29) Lee, J. K.; Walker, K. L.; Han, H. S.; Kang, J.; Prinz, F. B.; Waymouth, R. M.; Nam, H. G.; Zare, R. N. Spontaneous generation of hydrogen peroxide from aqueous microdroplets. *Proc. Natl. Acad. Sci. U.S.A.* **2019**, *116* (39), 19294−19298.
(30) Mehrgardi, M. A.; Mofidfar, M.; Zare, R. N. Sprayed water microdroplets are able to generate hydrogen peroxide spontaneously. *J. Am. Chem. Soc.* **2022**, *144* (17), 7606−7609.
(31) Lee, J. K.; Samanta, D.; Nam, H. G.; Zare, R. N. Spontaneous formation of gold nanostructures in aqueous microdroplets. *Nat. Commun.* **2018**, *9* (1), 1562.
(32) Xing, D.; Yuan, X.; Liang, C.; Jin, T.; Zhang, S.; Zhang, X. Spontaneous oxidation of I^- in water microdroplets and its atmospheric implications. *Chem. Commun.* **2022**, *58* (89), 12447−12450.
(33) Ruiz-Lopez, M. F.; Francisco, J. S.; Martins-Costa, M. T. C.; Anglada, J. M. Molecular reactions at aqueous interfaces. *Nat. Rev. Chem* **2020**, *4* (9), 459−475.
(34) Deal, A. M.; Rapf, R. J.; Vaida, V. Water-air interfaces as environments to address the water paradox in prebiotic chemistry: A physical chemistry perspective. *J. Phys. Chem. A* **2021**, *125* (23), 4929−4942.
(35) Li, K.; Wang, L.; Liu, J.; Gong, K.; Wang, W.; Ge, Q.; Liu, Y.; Zhang, L. A protocol to study microdroplet photoreaction at an individual droplet level using in situ micro-Raman spectroscopy. *STAR Protocols* **2022**, *3* (4), 101704.
(36) Huang, D.; Yin, L.; Niu, J. Photoinduced hydrodefluorination mechanisms of perfluorooctanoic acid by the SiC/graphene catalyst. *Environ. Sci. Technol.* **2016**, *50* (11), 5857−5863.
(37) Xiong, H.; Lee, J. K.; Zare, R. N.; Min, W. Strong electric field observed at the interface of aqueous microdroplets. *J. Phys. Chem. Lett.* **2020**, *11* (17), 7423−7428.
(38) Xiong, H.; Lee, J. K.; Zare, R. N.; Min, W. Strong concentration enhancement of molecules at the interface of aqueous microdroplets. *J. Phys. Chem. B* **2020**, *124* (44), 9938−9944.
(39) Ao, J.; Fang, X.; Miao, X.; Ling, J.; Kang, H.; Park, S.; Wu, C.; Ji, M. Switchable stimulated Raman scattering microscopy with photochromic vibrational probes. *Nat. Commun.* **2021**, *12* (1), 3089.

(40) Ao, J.; Feng, Y.; Wu, S.; Wang, T.; Ling, J.; Zhang, L.; Ji, M. Rapid, 3D chemical profiling of individual atmospheric aerosols with stimulated Raman scattering microscopy. *Small Methods* **2020**, *4* (2), 1900600.
(41) Wang, W.; Liu, M.; Wang, T.; Song, Y.; Zhou, L.; Cao, J.; Hu, J.; Tang, G.; Chen, Z.; Li, Z.; et al. Sulfate formation is dominated by manganese-catalyzed oxidation of SO_2 on aerosol surfaces during haze events. *Nat. Commun.* **2021**, *12* (1), 1993.
(42) Shi, H.; Cai, Z.; Patrow, J.; Zhao, B.; Wang, Y.; Wang, Y.; Benderskii, A.; Dawlaty, J.; Cronin, S. B. Monitoring local electric fields at electrode surfaces using surface enhanced Raman scattering-based stark-shift spectroscopy during hydrogen evolution reactions. *ACS Appl. Mater. Interfaces* **2018**, *10* (39), 33678−33683.
(43) Wu, Z.; Zhang, Y.; Zhang, L.; Zhou, B.; Wei, Z.; Wang, D.; Lu, W.; Jia, J.; Tao, L.; Wang, T.; et al. Coupling Fe(II)/Fe(III) redox mediated SO_2 conversion with hydrogen production. *Adv. Funct. Mater.* **2023**, *33*, 2212479.
(44) Song, Z.; Tang, H.; Wang, N.; Zhu, L. Reductive defluorination of perfluorooctanoic acid by hydrated electrons in a sulfite-mediated UV photochemical system. *J. Hazard. Mater.* **2013**, *262*, 332−338.
(45) Yuan, Y.; Feng, L.; Xie, N.; Zhang, L.; Gong, J. Rapid photochemical decomposition of perfluorooctanoic acid mediated by a comprehensive effect of nitrogen dioxide radicals and Fe^{3+}/Fe^{2+} redox cycle. *J. Hazard. Mater.* **2020**, *388*, 121730.
(46) Dall'Osto, M.; Beddows, D. C. S.; Harrison, R. M.; Onat, B. Fine iron aerosols are internally mixed with nitrate in the urban European atmosphere. *Environ. Sci. Technol.* **2016**, *50* (8), 4212−4220.
(47) Zhu, D.; Sun, Z.; Zhang, H.; Zhang, A.; Zhang, Y.; Miruka, A. C.; Zhu, L.; Li, R.; Guo, Y.; Liu, Y. Reactive nitrogen species generated by gas-liquid dielectric barrier discharge for efficient degradation of perfluorooctanoic acid from water. *Environ. Sci. Technol.* **2022**, *56* (1), 349−360.
(48) Goss, K. The pKa values of PFOA and other highly fluorinated carboxylic acids. *Environ. Sci. Technol.* **2008**, *42* (2), 456−458.
(49) Li, K.; Gong, K.; Liu, J.; Ohnoutek, L.; Ao, J.; Liu, Y.; Chen, X.; Xu, G.; Ruan, X.; Cheng, H.; et al. Significantly accelerated photochemical and photocatalytic reactions in microdroplets. *Cell Rep. Phys. Sci.* **2022**, *3*, 100917.
(50) Lin, J.; Hu, C.; Lo, S. Effect of surfactants on the degradation of perfluorooctanoic acid (PFOA) by ultrasonic (US) treatment. *Ultrason. Sonochem.* **2016**, *28*, 130−135.
(51) Li, Y.; Chien, W.; Liu, Y.; Lee, Y.; Lo, S.; Hu, C. Perfluorooctanoic acid (PFOA) removal by flotation with cationic surfactants. *Chemosphere* **2021**, *266*, 128949.
(52) Zhang, D.; Yuan, X.; Gong, C.; Zhang, X. High electric field on water microdroplets catalyzes spontaneous and ultrafast oxidative C-H/N-H cross-coupling. *J. Am. Chem. Soc.* **2022**, *144* (35), 16184−16190.
(53) Wei, Z.; Li, Y.; Cooks, R. G.; Yan, X. Accelerated reaction kinetics in microdroplets: Overview and recent developments. *Annu. Rev. Phys. Chem.* **2020**, *71* (1), 31−51.
(54) Lin, L.; Husek, J.; Biswas, S.; Baumler, S. M.; Adel, T.; Ng, K. C.; Baker, L. R.; Allen, H. C. Iron(III) speciation observed at aqueous and glycerol surfaces: Vibrational sum frequency and X-ray. *J. Am. Chem. Soc.* **2019**, *141* (34), 13525−13535.
(55) Huang, D.; Wang, J.; Xia, H.; Zhang, Y.; Bao, F.; Li, M.; Chen, C.; Zhao, J. Enhanced photochemical volatile organic compounds release from fatty acids by surface-enriched Fe(III). *Environ. Sci. Technol.* **2020**, *54* (21), 13448−13457.
(56) Tian, C.; Byrnes, S. J.; Han, H. L.; Shen, Y. R. Surface propensities of atmospherically relevant ions in salt solutions revealed by phase-sensitive sum frequency vibrational spectroscopy. *J. Phys. Chem. Lett.* **2011**, *2* (15), 1946−1949.
(57) Richards, N. K.; Wingen, L. M.; Callahan, K. M.; Nishino, N.; Kleinman, M. T.; Tobias, D. J.; Finlayson-Pitts, B. J. Nitrate ion photolysis in thin water films in the presence of bromide ions. *J. Phys. Chem. A* **2011**, *115* (23), 5810−5821.
(58) Wei, H.; Vejerano, E. P.; Leng, W.; Huang, Q.; Willner, M. R.; Marr, L. C.; Vikesland, P. J. Aerosol microdroplets exhibit a stable pH gradient. *Proc. Natl. Acad. Sci. U.S.A.* **2018**, *115* (28), 7272−7277.
(59) Hao, H.; Leven, I.; Head-Gordon, T. Can electric fields drive chemistry for an aqueous microdroplet? *Nat. Commun.* **2022**, *13* (1), 280.
(60) Mamatkulov, S. I.; Allolio, C.; Netz, R. R.; Bonthuis, D. J. Orientation-induced adsorption of hydrated protons at the air-water interface. *Angew. Chem., Int. Ed.* **2017**, *56* (50), 15846−15851.
(61) Sagar, D.; Bain, C. D.; Verlet, J. R. Hydrated electrons at the water/air interface. *J. Am. Chem. Soc.* **2010**, *132* (20), 6917−6919.
(62) Ren, B.; Huang, Q.; Xie, Y.; Tian, Z. Analyzing the adsorption behavior of thiocyanide on pure Pt and Ni electrode surfaces by confocal microprobe Raman spectroscopy. *Anal. Sci.* **2000**, *16* (2), 225−230.
(63) Chamberlayne, C. F.; Zare, R. N. Simple model for the electric field and spatial distribution of ions in a microdroplet. *J. Chem. Phys.* **2020**, *152* (18), 184702.
(64) Vogel, Y. B.; Evans, C. W.; Belotti, M.; Xu, L.; Russell, I. C.; Yu, L.-J.; Fung, A. K. K.; Hill, N. S.; Darwish, N.; Gonçales, V. R.; et al. The corona of a surface bubble promotes electrochemical reactions. *Nat. Commun.* **2020**, *11* (1), 6323.
(65) Wang, J.; Cao, C.; Zhang, Y.; Zhang, Y.; Zhu, L. Underneath mechanisms into the super effective degradation of PFOA by BiOF nanosheets with tunable oxygen vacancies on exposed (101) facets. *Appl. Catal., B* **2021**, *286*, 119911.
(66) Psillakis, E.; Cheng, J.; Hoffmann, M. R.; Colussi, A. J. Enrichment factors of perfluoroalkyl oxoanions at the air/water interface. *J. Phys. Chem. A* **2009**, *113* (31), 8826−8829.
(67) Wingen, L. M.; Moskun, A. C.; Johnson, S. N.; Thomas, J. L.; Roeselová, M.; Tobias, D. J.; Kleinman, M. T.; Finlayson-Pitts, B. J. Enhanced surface photochemistry in chloride-nitrate ion mixtures. *Phys. Chem. Chem. Phys.* **2008**, *10* (37), 5668−5677.
(68) Rana, B.; Fairhurst, D. J.; Jena, K. C. Investigation of water evaporation process at air/water interface using hofmeister ions. *J. Am. Chem. Soc.* **2022**, *144* (39), 17832−17840.
(69) Jungwirth, P.; Tobias, D. J. Molecular structure of salt solutions: A new view of the interface with implications for heterogeneous atmospheric chemistry. *J. Phys. Chem. B* **2001**, *105* (43), 10468−10472.
(70) Wu, X.; Lin, Y.; Wang, Y.; Wu, S.; Li, X.; Yang, C. Enhanced removal of hydrophobic short-chain n-alkanes from gas streams in biotrickling filters in presence of surfactant. *Environ. Sci. Technol.* **2022**, *56* (14), 10349−10360.
(71) Liu, X.; Liu, Y.; Qin, H.; Ye, Z.; Wei, X.; Miao, W.; Yang, D.; Mao, S. Selective removal of phenolic compounds by peroxydisulfate activation: Inherent role of hydrophobicity and interface ROS. *Environ. Sci. Technol.* **2022**, *56* (4), 2665−2676.
(72) Jiang, X.; Rotily, L.; Villermaux, E.; Wang, X. Submicron drops from flapping bursting bubbles. *Proc. Natl. Acad. Sci. U.S.A.* **2022**, *119* (1), No. e2112924119.

https://doi.org/10.1021/acs.est.3c05470
Environ. Sci. Technol. 2023, 57, 21448−21458